Inorganic Chemistry

Article

Cite This: Inorg. Chem. 2018, 57, 231−240

pubs.acs.org/IC

DFT Investigation of Ligand Photodissociation in $[Ru^{II}(tpy)(bpy)(py)]^{2+}$ and $[Ru^{II}(tpy)(Me_2bpy)(py)]^{2+}$ Complexes

Khalin Nisbett,[†] Yi-Jung Tu,[†] Claudia Turro,[‡] Jeremy J. Kodanko,[†] and H. Bernhard Schlegel*[,†]

[†]Department of Chemistry, Wayne State University, 5101 Cass Avenue, Detroit, Michigan 48202, United States

[‡]Department of Chemistry, The Ohio State University, Columbus, Ohio 43210, United States

Supporting Information

ABSTRACT: Photoinduced ligand dissociation of pyridine occurs much more readily in $[Ru(tpy)(Me_2bpy)(py)]^{2+}$ than in $[Ru(tpy)(bpy)(py)]^{2+}$ (tpy = 2,2′:6′,2″-terpyridine; bpy = 2,2′-bipyridine, Me_2bpy = 6,6′-dimethyl-2,2′-bipyridine; py = pyridine). The S_0 ground state and the ^{3}MLCT and ^{3}MC excited states of these complexes have been studied using BP86 density functional theory with the SDD basis set and effective core potential on Ru and the 6-31G(d) basis set for the rest of the atoms. In both complexes, excitation by visible light and intersystem crossing leads to a ^{3}MLCT state in which an electron from a Ru d orbital has been promoted to a π^* orbital of terpyridine, followed by pyridine release after internal conversion to a dissociative ^{3}MC state. Interaction between the methyl groups and the other ligands causes significantly more strain in $[Ru(tpy)(Me_2bpy)(py)]^{2+}$ than in $[Ru(tpy)(bpy)(py)]^{2+}$, in both the S_0 and ^{3}MLCT states. Transition to the dissociative ^{3}MC states releases this strain, resulting in lower barriers for ligand dissociation from $[Ru(tpy)(Me_2bpy)(py)]^{2+}$ than from $[Ru(tpy)(bpy)(py)]^{2+}$. Analysis of the molecular orbitals along relaxed scans for stretching the Ru−N bonds reveals that ligand photodissociation is promoted by orbital mixing between the ligand π^* orbital of tpy in the ^{3}MLCT state and the dσ^* orbitals that characterize the dissociative ^{3}MC states. Good overlap and strong mixing occur when the Ru−N bond of the leaving ligand is perpendicular to the π^* orbital of terpyridine, favoring the release of pyridine positioned in a *cis* fashion to the terpyridine ligand.

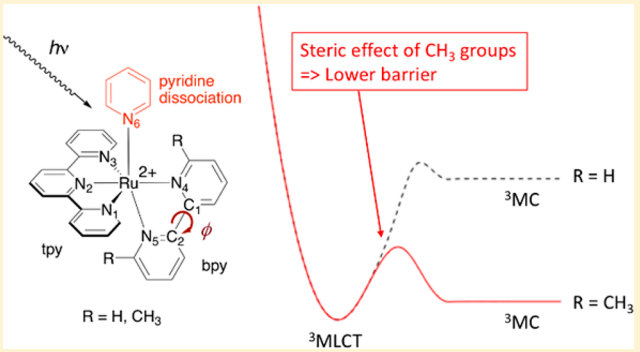

INTRODUCTION

There is a highly sustained interest in photoactivatable metal complexes for applications in the broad field of solar energy conversion, including the photocatalytic production of fuels from abundant sources and photovoltaic systems, as well as compounds that have increasing potential as tools in biomedical research.[1−5] Photoactivated compounds that release biologically active species from a nontoxic metal-based chaperone in the presence of light are being developed, so that the release can be accomplished with spatiotemporal control over biological activity. Their potential as selective and specific tools for biological research as well as agents for photoactivated chemotherapy (PACT) has been noted.[6−12]

Photoinduced therapies are being developed for the treatments of various disease states, including cancer and microbial infections.[4−14] Active species currently being used include established inhibitors, neurotransmitters, drugs, and their derivatives.[15−17] Therapies that rely on photoactivation overcome the downfalls of those that are currently in use which lack the ability to achieve location-specific inhibition and have low bioavailability, leading to dose escalation, drug resistance, and intensified side effects.[18] A photoreleasable drug or inhibitor has the potential to minimize the risk and side effects by providing noninvasive methods for achieving high levels of control over the effects of drugs in diseased vs normal tissue.

Metal centers of interest include Pt(IV),[19] Re(I),[20] and Ir(III)[21] as well as complexes containing Ru(II), which have all been investigated extensively. Photoactivatable Ru(II)-centered chaperones are typically composed of tridentate or bidentate chelators, such as 2,2′:6′,2″-terpyridine (tpy), 2,2′-bipyridine (bpy), and 1,10-phenanthroline (phen) and their derivatives as ancillary ligands and one or more monodentate ligands as the active species for release. The low ligand exchange in Ru(II) complexes observed in the dark, together with their high photoreactivity, makes these complexes highly attractive as potential PACT agents. In photochemotherapy, absorption of a photon by the complex opens coordination sites on the ruthenium for binding to biomolecules, including DNA and proteins. Alternatively, the photodissociation can be used to release reactive molecules and species while the leftover ruthenium fragment is not toxic, which is a highly desirable property for chemical tools. The efficiency of a PACT agent is typically rated on the basis of its relative efficacy upon irradiation in comparison to dark conditions. Chaperone complexes that

Received: September 20, 2017
Published: December 19, 2017

DOI: 10.1021/acs.inorgchem.7b02398
Inorg. Chem. 2018, 57, 231−240

can release two or three monodentate active nitrile species have also been previously developed.[4,22,23] In these compounds, only one of the biologically active ligands usually dissociates efficiently upon irradiation.

Whereas much of the initial work in the field focused on the photorelease of nitrile-bound inhibitors and drugs, the Turro group recently designed a photoactive Ru(II) complex able to deliver pyridine and pyridine-bound inhibitors efficiently with low-energy visible light, a requirement for tissue penetration.[24] The release of pyridine and other N-heterocycles is important due to the very large number of active agents available that contain these functional groups, opening the field of PACT to include compounds that can achieve a method of cell death independent of oxygen concentration,[12] unlike the case for photodynamic therapy, which requires oxygen. When the octahedral orientation is distorted using 6,6′-dimethyl-2,2′-bipyridine (Me_2bpy), these complexes become more photoreactive. $[Ru(tpy)(bpy)(py)]^{2+}$ and $[Ru(tpy)(Me_2bpy)(py)]^{2+}$ complexes (Scheme 1) are stable in the dark, and the latter releases pyridine efficiently upon irradiation with visible light, whereas pyridine ligand exchange is not observed in the former upon photoexcitation under the same conditions.[25]

It is generally accepted that photoactivated dissociation and solvolysis occurs because a dissociative triplet metal-centered state is thermally accessible from the observed triplet metal−ligand charge transfer state.[25−37] Through steric crowding about the Ru center, the $Ru-N_5$ and $Ru-N_6$ bonds are distorted in $[Ru(tpy)(Me_2bpy)(py)]^{2+}$ relative to $[Ru(tpy)(bpy)(py)]^{2+}$. As a result, the energy difference between the ^{3}MC and ^{3}MLCT states is smaller in $Ru(tpy)(Me_2bpy)(py)]^{2+}$, allowing for efficient population of the ^{3}MC state and increase

Scheme 1. $[Ru(tpy)(bpy)(py)]^{2+}$ and $[Ru(tpy)(Me_2bpy)(py)]^{2+}$ Complexes with Atomic Numbering

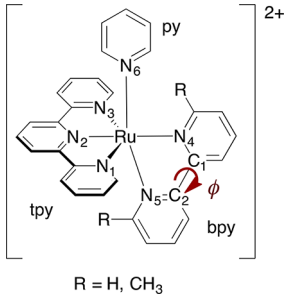

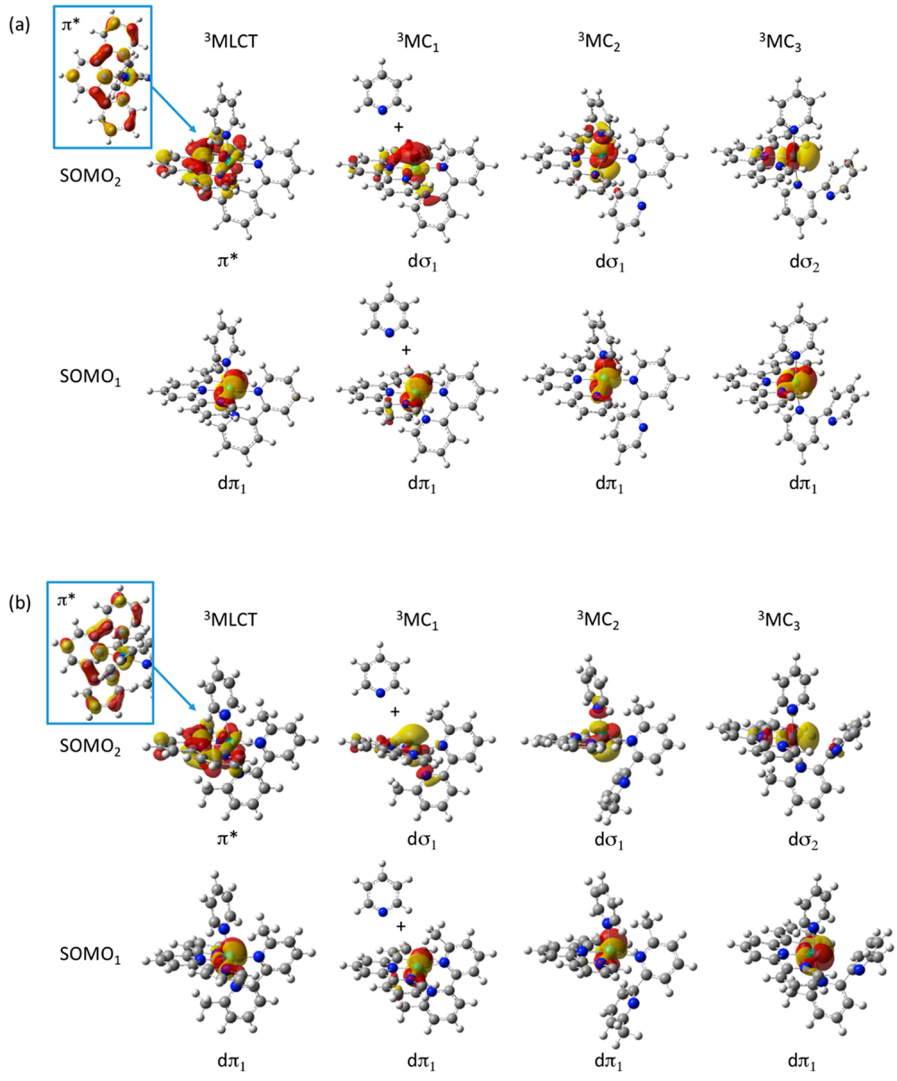

Figure 1. Biorthogonal orbitals of $SOMO_1$ and $SOMO_2$ for the ^{3}MLCT and ^{3}MC states of (a) $[Ru(tpy)(bpy)(py)]^{2+}$ and (b) $[Ru(tpy)(Me_2bpy)(py)]^{2+}$. Higher resolution plots of the biorthogonal and canonical SOMOs are available in Figure S1 and S2 of the Supporting Information.

DOI: 10.1021/acs.inorgchem.7b02398
Inorg. Chem. 2018, 57, 231−240

in the quantum yield for photodissociation. In $[Ru(tpy)(bpy)(py)]^{2+}$,[29,34] population of the ^{3}MC state and photodissociation are unfavorable because the ^{3}MC state is significantly higher in energy than the ^{3}MLCT state.

For biomedical applications, it is desirable for the complex to absorb red or near-IR wavelengths of light, which penetrate tissue more deeply than shorter wavelengths in the visible and UV regions. It is also necessary that excitation is followed by conversion to an excited state that will promote ligand dissociation. In Ru(II) complexes, excitation to a singlet metal−ligand charge transfer state (^{1}MLCT) state is followed by ultrafast intersystem crossing to a triplet metal−ligand charge transfer state (^{3}MLCT), and the dissociative triplet metal-centered state (^{3}MC) is known to be thermally accessible from the ^{3}MLCT state.[26−37] In $[Ru(tpy)(Me_2bpy)(py)]^{2+}$, photodissociation consistently leads to the substitution of the pyridine ligand by coordinating solvent molecules. In a previous study, we developed a molecular orbital based explanation for the selectivity of photochemical ligand dissociation in ruthenium nitrile complexes.[38] When the orbitals are oriented favorably, mixing between the ligand π^* orbital and the Ru $d\sigma^*$ orbital was shown to lead to a low barrier for the conversion of the ^{3}MLCT state to a dissociative ^{3}MC state. The same mechanism explains the selective ligand release in ruthenium tris(2-pyridylmethyl)amine (tpa) complexes. These prior findings motivated us to explore the photodissociation of pyridine in $[Ru(tpy)(bpy)(py)]^{2+}$ and $[Ru(tpy)(Me_2bpy)(py)]^{2+}$ complexes, the subject of the present work.

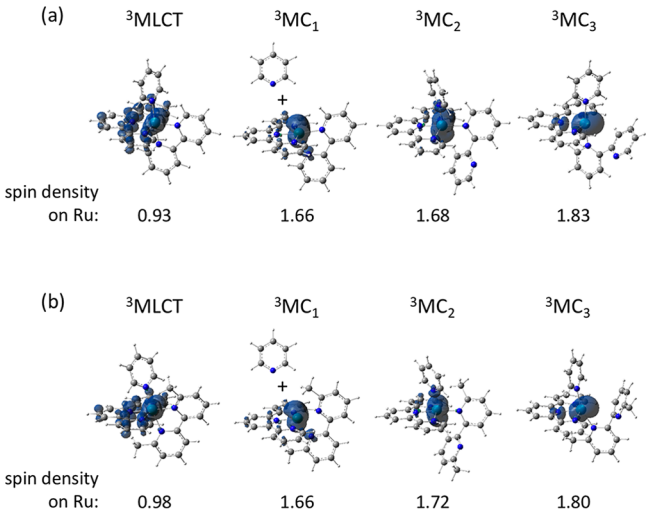

Figure 2. Spin density plots for the ^{3}MLCT and ^{3}MC states of (a) $[Ru(tpy)(bpy)(py)]^{2+}$ and (b) $[Ru(tpy)(Me_2bpy)(py)]^{2+}$.

COMPUTATIONAL METHODS

Electronic structure calculations were performed using Gaussian 09[39] and the BP86 density functional.[40,41] For a set of Ru(II) polypyridyl complexes, Gonzalez and co-workers[42] found that BP86 showed the best state ordering and state mixing in comparison to MS-CASPT2 calculations. In preparation for our earlier study,[38] we examined a number of different functionals and found that the ^{3}MC state of a RuTQA complex was 3−27 kcal/mol lower in energy than the ^{3}MLCT state. The BP86 functional gave the smallest energy difference between the ^{3}MLCT and ^{3}MC states, whereas the hybrid functionals gave the largest energy differences. The SDD basis set and effective core potential[43−45] were used for the central Ru atom. The 6-31G(d) basis set[46,47] was used for the other atoms. Solvation effects in methanol were incorporated by using the implicit SMD solvation model[48] and were included during structure optimization. The optimized structures were confirmed to be minima by harmonic vibrational frequency calculations. The ^{1}S$_0$, ^{3}MLCT, and ^{3}MC electronic configurations were tested for SCF stability and were characterized by examining the molecular orbital populations and the spin densities. GaussView[49] was used to generate isodensity plots of the spin densities (isovalue 0.004 au), the canonical orbitals, and biorthogonal/corresponding orbitals[50] (isovalue 0.04 au). To explore the potential energy surfaces for dissociation, relaxed potential energy surface scans were performed by stretching selected Ru−N bonds while the remaining coordinates were optimized. Transition states were obtained by optimizing the highest energy structures of the relaxed scans and were confirmed to have only one imaginary vibrational frequency.

RESULTS AND DISCUSSION

The photoinduced ligand dissociation in the $[Ru(tpy)(bpy)(py)]^{2+}$ and $[Ru(tpy)(Me_2bpy)(py)]^{2+}$ complexes (Scheme 1) has been studied experimentally and reported previously.[24,34] Upon irradiation with visible light, the pyridine ligand

Table 1. Selected Calculated Bond Distances (Å) and Angles (deg) for $[Ru(tpy)(bpy)(py)]^{2+}$ and $[Ru(tpy)(Me_2bpy)(py)]^{2+}$ Complexes in the S$_0$, ^{3}MLCT, ^{3}MC, and ^{3}TS States in Methanol

	Ru−N$_1$	Ru−N$_2$	Ru−N$_3$	Ru−N$_4$	Ru−N$_5$	Ru−N$_6$	N$_1$−Ru−N$_3$	N$_2$−Ru−N$_4$	N$_5$−Ru−N$_6$	ϕ^c
					$[Ru(tpy)(bpy)(py)]^{2+}$					
S$_0$	2.080	1.979	2.088	2.094	2.070	2.130	158.7	175.1	172.6	−2.4
^{3}MLCT	2.086	2.031	2.081	2.103	2.088	2.125	151.8	175.8	175.7	−2.1
^{3}MC$_1$[a]	2.096	1.987	2.097	2.095	2.171		157.1	174.0		1.5
^{3}MC$_2$	2.137	2.006	2.090	2.160	4.593	2.215	146.2	175.2	127.5	−141.8
^{3}MC$_3$	2.120	2.203	2.131	4.384	2.142	2.125	147.0	135.9	170.8	137.2
^{3}TS$_1$[b]	2.097	1.985	2.087	2.115	2.170	3.036	155.0	172.2	163.0	2.7
					$[Ru(tpy)(Me_2bpy)(py)]^{2+}$					
S$_0$	2.073	1.979	2.106	2.124	2.126	2.132	158.3	179.1	168.3	−1.4
^{3}MLCT	2.084	2.039	2.120	2.131	2.169	2.119	149.6	176.2	169.0	−0.1
^{3}MC$_1$[a]	2.088	1.982	2.095	2.124	2.225		154.8	166.0		2.5
^{3}MC$_2$	2.151	2.000	2.075	2.197	4.246	2.261	148.2	169.6	132.0	−134.2
^{3}MC$_3$	2.115	2.165	2.118	3.961	2.179	2.152	146.0	152.0	157.3	117.4
^{3}TS$_1$[b]	2.100	1.993	2.111	2.156	2.182	2.639	154.5	173.8	165.5	−7.6
^{3}TS$_2$[b]	2.095	1.990	2.151	2.169	2.439	2.691	149.8	177.7	152.5	−18.8

[a]Five-coordinate ^{3}MC$_1$ structure that has released the pyridine. [b]Optimized transition structures are shown in Figure 5. [c]Dihedral angle ϕ is defined in Scheme 1.

DOI: 10.1021/acs.inorgchem.7b02398
Inorg. Chem. 2018, 57, 231−240

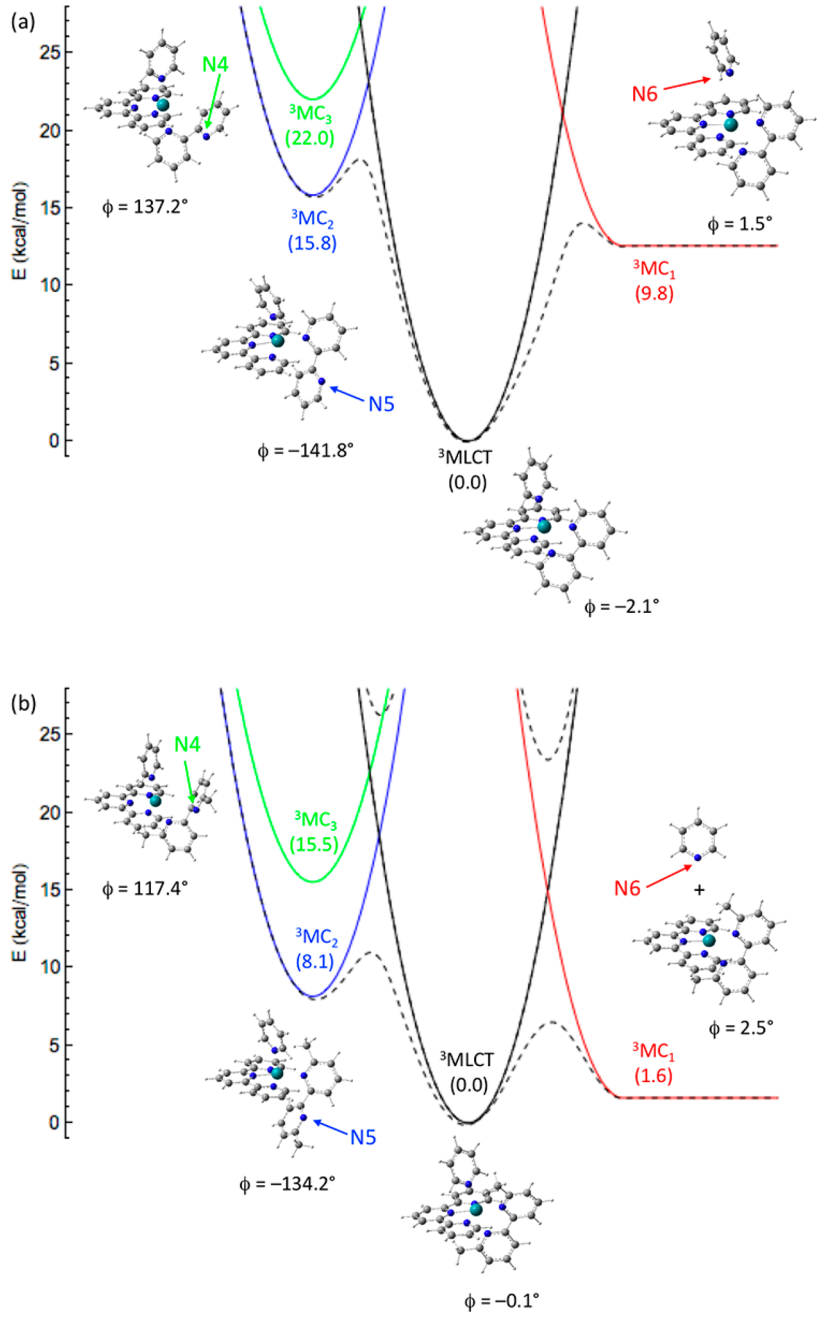

Figure 3. Relative energies of the ^{3}MLCT and ^{3}MC structures for (a) $[Ru(tpy)(bpy)(py)]^{2+}$ and (b) $[Ru(tpy)(Me_2bpy)(py)]^{2+}$. The arrows indicate the positions of ligand dissociation. The definition of dihedral angle ϕ is shown in Scheme 1.

dissociates from $[Ru(tpy)(Me_2bpy)(py)]^{2+}$ much more readily than from $[Ru(tpy)(bpy)(py)]^{2+}$, and in fact, ligand exchange from the latter is not observed under certain irradiation conditions. Typically, the ^{1}MLCT excited states of Ru complexes convert rapidly to a lower ^{3}MLCT state by intersystem crossing. It is generally accepted that ligand dissociation occurs via internal conversion of the ^{3}MLCT states to a dissociative ^{3}MC state.[25−37] Therefore, exploration of the triplet potential energy surface is key to the understanding of the photodissociative behavior of these Ru complexes. The molecular orbitals and spin densities for the lowest ^{3}MLCT and the three lowest ^{3}MC states of the $[Ru(tpy)(bpy)(py)]^{2+}$ and $[Ru(tpy)(Me_2bpy)(py)]^{2+}$ complex are shown in Figures 1 and 2 and in Figures S1 and S2 of the Supporting Information.

The difference between the ^{3}MLCT and ^{3}MC states can be discerned from the singly occupied molecular orbitals (SOMOs) and from the different spin densities on Ru. For the ^{3}MLCT state, SOMO$_1$ is a dπ orbital of Ru and SOMO$_2$ is a π^* orbital of the tpy ligand, resulting in Mulliken spin densities of 0.93 and 0.98 on Ru for $[Ru(tpy)(bpy)(py)]^{2+}$ and $[Ru(tpy)(Me_2bpy)(py)]^{2+}$, respectively. The two unpaired electrons in the ^{3}MC states occupy a dπ orbital and a dσ^* orbital on Ru, yielding spin densities on Ru ranging from 1.66 to 1.83 for ^{3}MC$_1$, ^{3}MC$_2$, and ^{3}MC$_3$ for the two complexes. Because the SOMOs of the ^{3}MC states have dσ^* antibonding character in Ru−N bonds, the various ^{3}MC states can be found by elongating different Ru−N bonds in the ^{3}MLCT excited state structure. The nature of these ^{3}MC states can be understood in terms of the different Ru d orbitals involved in the

DOI: 10.1021/acs.inorgchem.7b02398
Inorg. Chem. 2018, 57, 231−240

SOMOs. In the $^3MC_1$ state, the Ru−N_6 bond dissociates and $SOMO_2$ is a dσ_1* orbital of Ru which is antibonding with N_5 and N_6, while $SOMO_1$ is a dπ_1 orbital of Ru (comparable to $SOMO_1$ of the ^3MLCT state). $SOMO_1$ and $SOMO_2$ in the $^3MC_2$ state are similar to those in $^3MC_1$, since the Ru−N_5 bond is elongated along the same axis as Ru−N_6. In the $^3MC_3$ state, the Ru−N_4 bond is broken, and $SOMO_2$ is a dσ_2* orbital of Ru which is antibonding with N_2 and N_4.

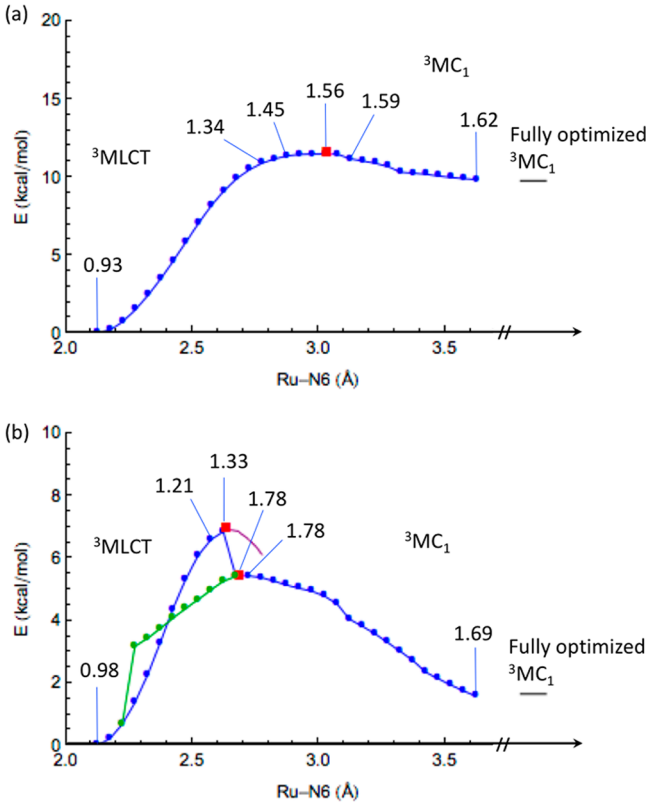

Figure 4. Relaxed potential energy scans from the ^3MLCT state for stretching the Ru−N_6 bond of (a) $[Ru(tpy)(bpy)(py)]^{2+}$ and (b) $[Ru(tpy)(Me_2bpy)(py)]^{2+}$. The red squares indicate the optimized transition states. The values along the scan show the spin densities on Ru. For (b), the purple line is the IRC in the forward direction from $^3TS_1$ and the green line is the relaxed scan in the reverse direction from Ru−N6 = 2.67 Å.

The Ru−N bond lengths in the S_0, ^3MLCT, and ^3MC states of $[Ru(tpy)(bpy)(py)]^{2+}$ and $[Ru(tpy)(Me_2bpy)(py)]^{2+}$ are compared in Table 1. Methyl substitution on the bpy ligand results in a more crowded structure and increases the calculated Ru−N_4 and Ru−N_5 bond lengths in the ground state.[24] Similar increases in these bond lengths are found in the excited-state structures. The changes in the N−Ru−N angles also reflect this crowding. Only modest changes in the bond lengths are seen on excitation from S_0 to ^3MLCT. The S_0 to ^3MLCT excitation energies for $[Ru(tpy)(bpy)(py)]^{2+}$ and $[Ru(tpy)(Me_2bpy)(py)]^{2+}$ are 41.8 and 40.4 kcal/mol, respectively, indicating that the methyl groups have similar effects on the S_0 and ^3MLCT states. Excitation to the ^3MLCT state puts an electron in the tpy π* orbital, and the nodal patterns of this orbital explain the bond length changes in the tpy ligand seen on excitation (see Table S1 in the Supporting Information).

Stretching the Ru−N_6 bond in the ^3MLCT optimized structure results in conversion to the $^3MC_1$ state. Geometry optimization of the $^3MC_1$ structure leads to a weakly bound six-coordinate structure which dissociates to a five-coordinate complex and a free pyridine that is about 2 kcal/mol higher in energy. Because $SOMO_2$ is a dσ* orbital aligned with both the Ru−N_6 and Ru−N_5 bonds, the latter is also somewhat elongated (Table 1). Figure 3 shows the relative energies of the optimized ^3MLCT and ^3MC structures. The six-coordinate $^3MC_1$ structure for $[Ru(tpy)(bpy)(py)]^{2+}$ is 9.8 kcal/mol higher in energy than the ^3MLCT state. For $[Ru(tpy)(Me_2bpy)(py)]^{2+}$; the five-coordinate $^3MC_1$ structure is only 1.6 kcal/mol higher in energy than the ^3MLCT state since elongation of the Ru−N_6 bond releases the strain from interaction between the pyridine and the methyl group of Me_2bpy.

Stretching of the Ru−bpy bonds leads to the $^3MC_2$ and $^3MC_3$ states. The $^3MC_2$ optimized structures are 15.8 and 8.1 kcal/mol higher in energy than the ^3MLCT states for $[Ru(tpy)(bpy)(py)]^{2+}$ and $[Ru(tpy)(Me_2bpy)(py)]^{2+}$, respectively. The difference can be attributed to the release of strain from interaction between tpy and the methyl group of Me_2bpy in the latter complex. In the $^3MC_2$ structure, the Ru−N_5 bond elongates and the N_5 pyridyl group of bpy rotates away from Ru.

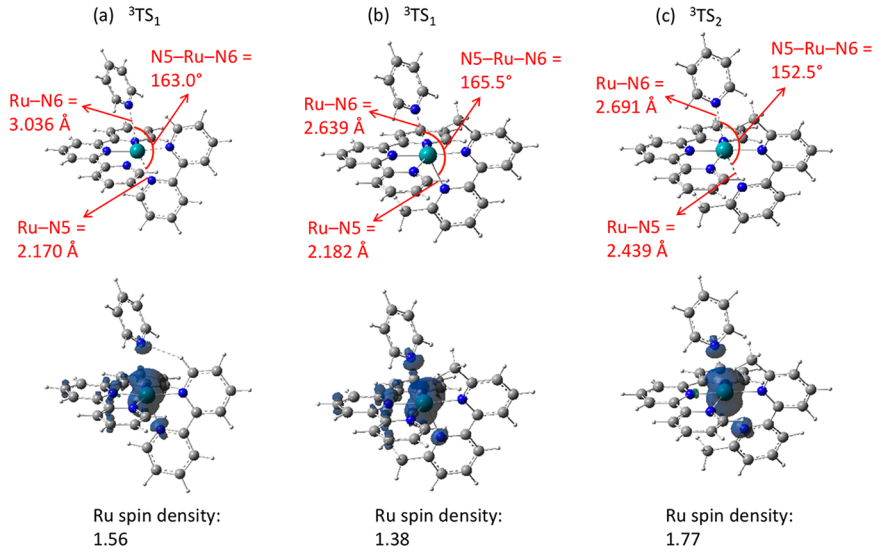

Figure 5. Optimized transition state geometries and spin density plots for the conversion from ^3MLCT to $^3MC_1$: (a) $^3TS_1$ for $[Ru(tpy)(bpy)(py)]^{2+}$; (b) $^3TS_1$ for $[Ru(tpy)(Me_2bpy)(py)]^{2+}$; (c) $^3TS_2$ for $[Ru(tpy)(Me_2bpy)(py)]^{2+}$.

DOI: 10.1021/acs.inorgchem.7b02398
Inorg. Chem. 2018, 57, 231−240

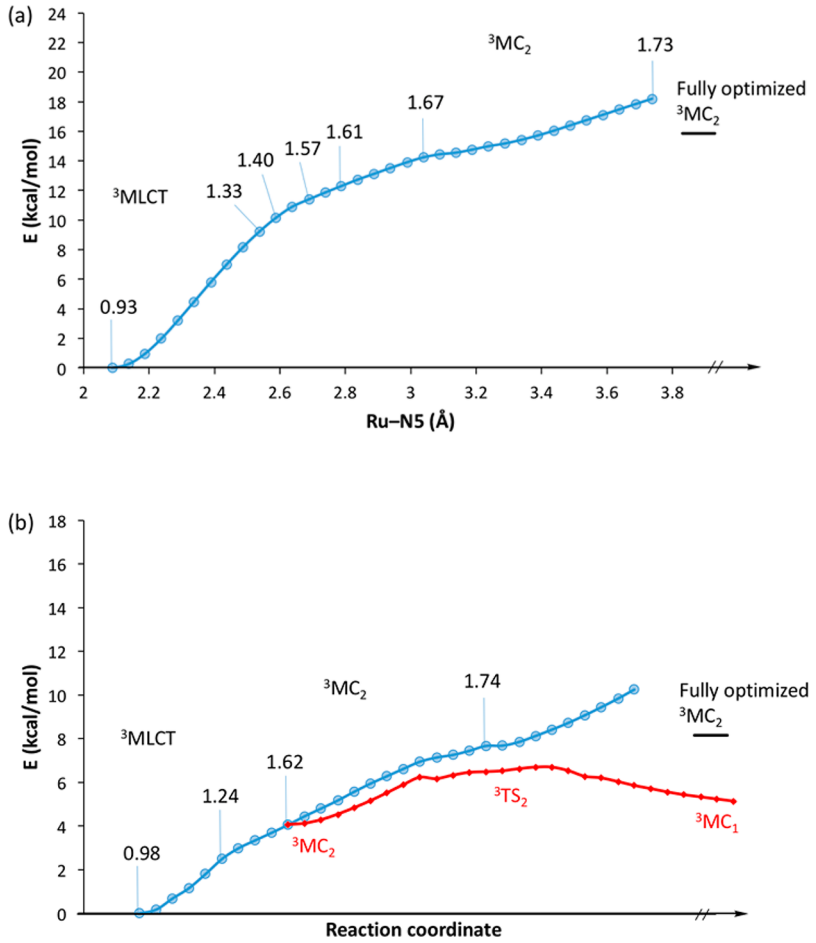

Figure 6. Relaxed potential energy scans from the ^{3}MLCT state for stretching the Ru–N_5 bond in (a) $[Ru(tpy)(bpy)(py)]^{2+}$ and (b) $[Ru(tpy)(Me_2bpy)(py)]^{2+}$. The red line represents the relaxed scan for stretching the Ru–N_6 bond in $[Ru(tpy)(Me_2bpy)(py)]^{2+}$ when the Ru–N_5 bond is frozen at 2.62 Å. The values along the scan show the spin densities on Ru.

For the ^{3}MC$_3$ structures, the N_4 pyridyl group of bpy rotates away from Ru, resulting in structures that are 22.0 and 15.5 kcal/mol higher than ^{3}MLCT for $[Ru(tpy)(bpy)(py)]^{2+}$ and $[Ru(tpy)(Me_2bpy)(py)]^{2+}$, respectively. The fact that ^{3}MC$_1$ is the lowest-energy ^{3}MC state is consistent with the experimental results that the ligand dissociation occurs at the N_6 position.

Potential Energy Scan on Triplet Surface. The energy barriers for the ligand dissociation on the triplet surface can be estimated by conducting relaxed scans from ^{3}MLCT and stretching various Ru–N bonds. For each scan, one Ru–N bond was chosen, elongated in steps of 0.05 Å, and the energy was minimized with respect to all of the remaining coordinates at each step of the scan. When the Ru–N_6 bond in $[Ru(tpy)(bpy)(py)]^{2+}$ is elongated, there is a smooth transition from the ^{3}MLCT to ^{3}MC$_1$ state with a barrier of approximately 12 kcal/mol (Figure 4a). After the barrier, there is a weakly bound six-coordinate complex before the pyridine fully dissociates to the five-coordinate ^{3}MC$_1$ complex. The transition state structure ^{3}TS$_1$ for $[Ru(tpy)(bpy)(py)]^{2+}$ (Figure 5a) was found by optimizing the highest energy point on the scan, yielding a barrier height of 11.5 kcal/mol.

When the Ru–N_6 bond in $[Ru(tpy)(Me_2bpy)(py)]^{2+}$ is elongated, the transition from the ^{3}MLCT to ^{3}MC$_1$ state occurs at a shorter distance and has a barrier of only approximately 7 kcal/mol (Figure 4b). Transition state ^{3}TS$_1$ for $[Ru(tpy)(Me_2bpy)(py)]^{2+}$ (Figure 5b) was found by optimizing the highest energy point on the scan. The optimized ^{3}TS$_1$ is 6.9 kcal/mol higher in energy than the ^{3}MLCT structure and has one imaginary frequency which corresponds to stretching of the Ru–N_6 bond. Following the IRC and the relaxed scan confirms that this transition state connects to the ^{3}MC$_1$ structure. Structure ^{3}TS$_1$ has a spin density of 1.38 on Ru (midway between 0.98 in ^{3}MLCT and 1.66 in ^{3}MC$_1$) and a Ru–N_6 bond length of 2.639 Å. The differences between $[Ru(tpy)(bpy)(py)]^{2+}$ and $[Ru(tpy)(Me_2bpy)(py)]^{2+}$ in both the barrier heights and the Ru–N_6 bond lengths can be understood in terms of an avoided crossing between the potential energy surfaces of the ^{3}MLCT and ^{3}MC$_1$ states as the Ru–N_6 bond is stretched (see Figure 3). Because the ^{3}MLCT to ^{3}MC$_1$ energy difference is smaller for $[Ru(tpy)(Me_2bpy)(py)]^{2+}$ than for $[Ru(tpy)(bpy)(py)]^{2+}$, the avoided crossing between the ^{3}MLCT and ^{3}MC$_1$ states occurs at a lower energy and shorter bond length for $[Ru(tpy)(Me_2bpy)(py)]^{2+}$. Other coordinates such as the Ru–N_5 bond length and various N–Ru–N angles also indicate that the transition state for $[Ru(tpy)(Me_2bpy)(py)]^{2+}$ occurs earlier along the reaction path with a greater release of strain in comparison to the transition state for $[Ru(tpy)(bpy)(py)]^{2+}$. Because the conversion of ^{3}MLCT to ^{3}MC involves electron transfer from the tpy ligand to Ru, some changes are also observed in the bond length of the tpy ligand (see Table S1 in the Supporting Information).

DOI: 10.1021/acs.inorgchem.7b02398
Inorg. Chem. 2018, 57, 231–240

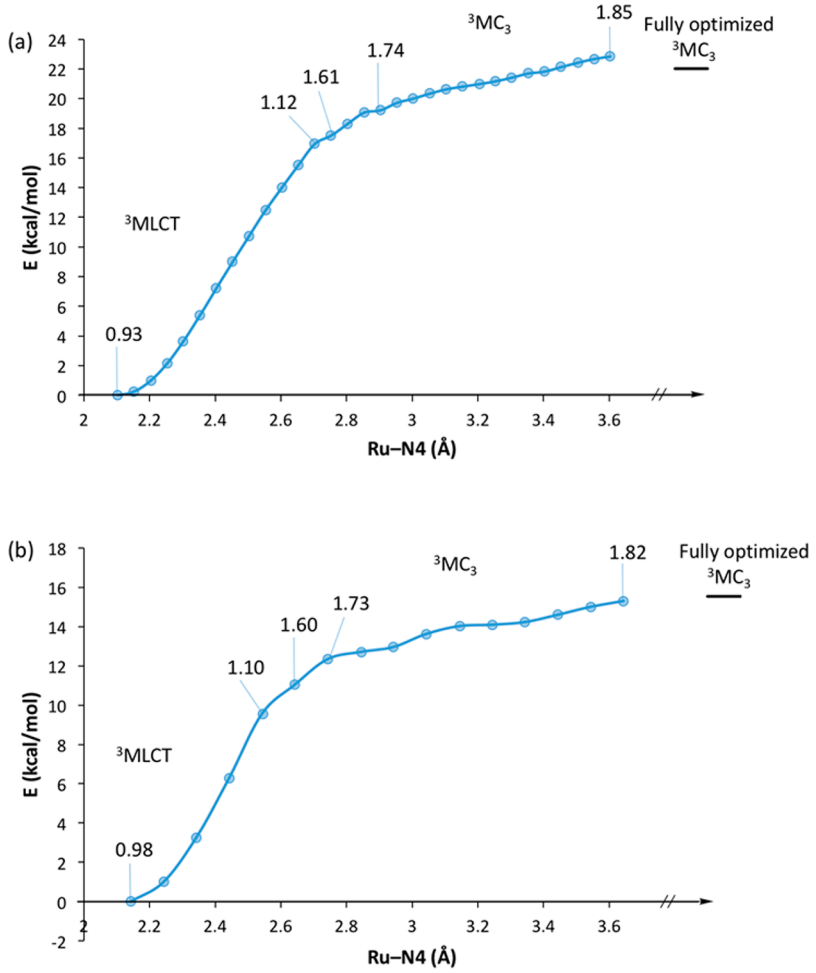

Figure 7. Relaxed potential energy scans from the ^{3}MLCT state for stretching the Ru–N$_4$ bond in (a) [Ru(tpy)(bpy)(py)]$^{2+}$ and (b) [Ru(tpy)(Me$_2$bpy)(py)]$^{2+}$. The values along the scan show the spin densities on Ru.

After the high point on the scan of the Ru–N$_6$ in [Ru(tpy)(Me$_2$bpy)(py)]$^{2+}$, there is a 1.4 kcal/mol drop in energy (Figure 4b) and a 0.298 Å lengthening of the Ru–N$_5$ bond (Figure S3 in the Supporting Information). Continuing the scan in the forward direction leads to the ^{3}MC$_1$ structure. The energy decreases monotonically while the Ru–N$_5$ bond shortens and the Me$_2$bpy ligand twists to a lower energy geometry. Scanning the Ru–N$_6$ bond in the reverse direction also produces a monotonic decrease in energy (Figure 4b, green line), leading to the ^{3}MLCT structure. Optimizing the highest energy point on this scan results in transition structure ^{3}TS$_2$ (Figure 5c), which is 5.4 kcal/mol above the ^{3}MLCT state. The Ru–N$_6$ bond length in ^{3}TS$_2$ is similar to that in ^{3}TS$_1$ but the Ru–N$_5$ bond length is significantly longer and the spin density on Ru is higher. As discussed in the next paragraph, ^{3}TS$_2$ can also be found by stretching the Ru–N$_5$ bond in the ^{3}MLCT structure and then stretching the Ru–N$_6$ bond. Thus, ^{3}TS$_2$ represents the barrier for a second, lower energy pathway for dissociation of the ^{3}MLCT state to form the ^{3}MC$_1$ and pyridine.

Elongation of the Ru–N$_5$ bond perpendicular to the tpy plane results in a smooth increase in the energy from the ^{3}MLCT state to the ^{3}MC$_2$ state (Figure 6). The increase for [Ru(tpy)(Me$_2$bpy)(py)]$^{2+}$ is significantly smaller than for [Ru(tpy)(bpy)(py)]$^{2+}$. When the Ru–N$_5$ bond in [Ru(tpy)-(Me$_2$bpy)(py)]$^{2+}$ is stretched to 2.62 Å, the potential energy increases by 4.05 kcal/mol, the spin density on Ru increases gradually to 1.62, and the Ru–N$_6$ bond elongates slightly to 2.26 Å. Because the bpy ligand is tethered to Ru at the N$_4$ position, the N$_5$ pyridyl does not dissociate. When the Ru–N$_5$ bond is stretched beyond 2.62 Å, the potential energy continues to increase because of the twisting of the bpy ligand. If the Ru–N$_5$ bond is frozen at 2.62 Å and another relaxed scan is conducted by stretching the Ru–N$_6$ bond, the energy increases monotonically until the pyridine dissociates. Optimization of the highest point on this scan results in transition state ^{3}TS$_2$ (Figure 5c).

When the Ru–N$_4$ bond, which is coplanar with the tpy ligand, is stretched, the estimated barrier for the transition to the ^{3}MC$_3$ state is 23 kcal/mol for [Ru(tpy)(bpy)(py)]$^{2+}$ and 15 kcal/mol for [Ru(tpy)(Me$_2$bpy)(py)]$^{2+}$, values that are significantly higher than for the conversion to the ^{3}MC$_1$ and ^{3}MC$_2$ states (Figure 7). The higher barriers for breaking the Ru–N$_4$ bond are consistent with experiment, which did not find photodissociation of the bpy ligand.

MO Analysis along the Relaxed Scans. In our previous study[38] we analyzed the SOMOs along the relaxed potential energy scans and found that photodissociation of the nitrile-bound Ru polypyridyl complexes is facilitated by orbital mixing between the ligand π^* orbital of the ^{3}MLCT state and the Ru dσ^* orbitals of a dissociative ^{3}MC state. Figure 8 shows the corresponding plots for the SOMOs of [Ru(tpy)(Me$_2$bpy)(py)]$^{2+}$ as

DOI: 10.1021/acs.inorgchem.7b02398
Inorg. Chem. 2018, 57, 231–240

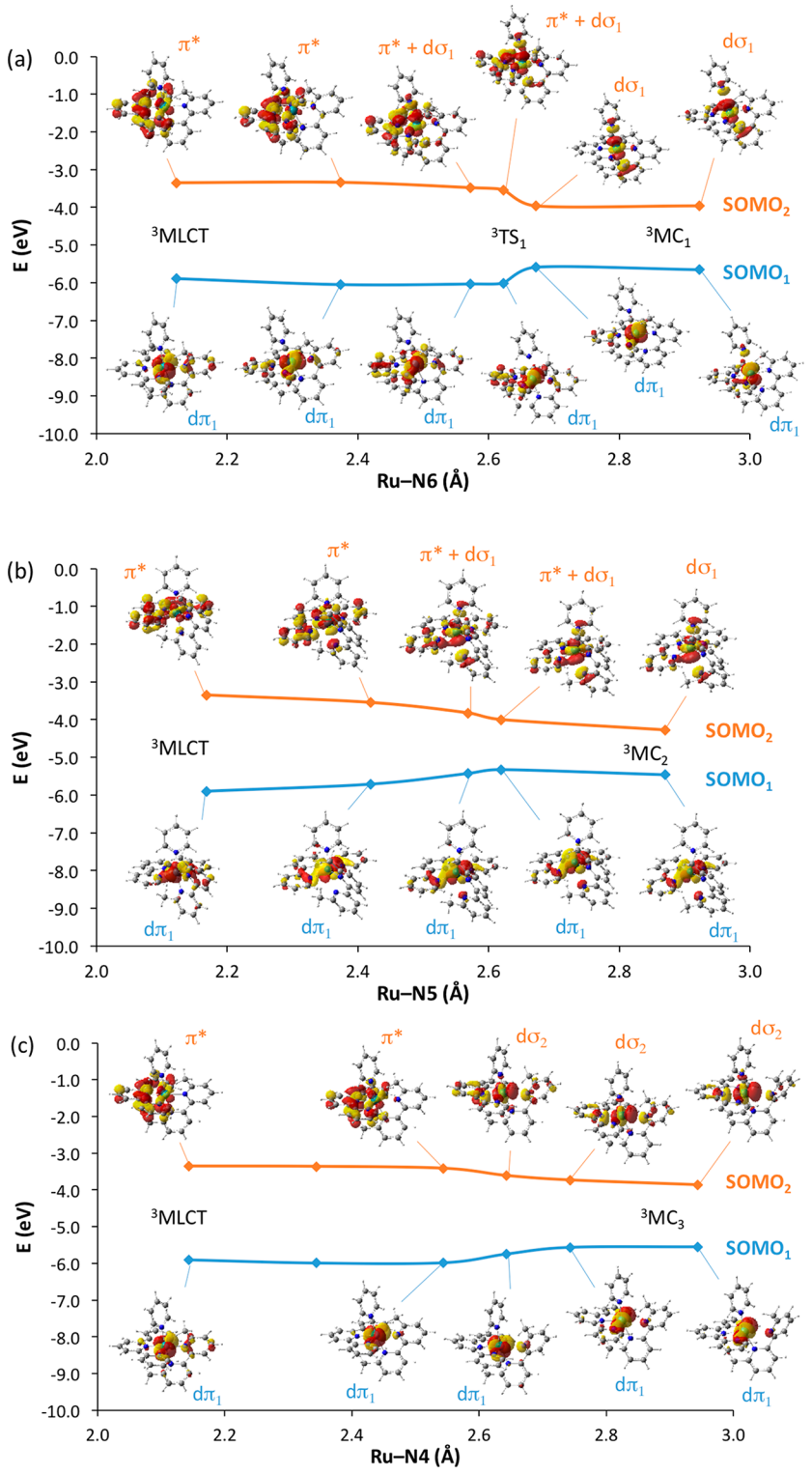

Figure 8. Isosurface plots of the SOMOs of $[Ru(tpy)(Me_2bpy)(py)]^{2+}$ along the relaxed scan of the ^{3}MLCT state for elongation of (a) Ru−N_6, (b) Ru−N_5, and (c) Ru−N_4.

the Ru−N_6, Ru−N_5, and Ru−N_4 bonds are stretched. $SOMO_2$ in the ^{3}MLCT state is a ligand-based π^* orbital on tpy. When the Ru−N_6 bond is stretched longer than 2.52 Å, the ligand-based $SOMO_2$ mixes with the $d\sigma_1^*$ orbital of Ru, which corresponds to $SOMO_2$ of $^3MC_1$ (Figure 8a). This orbital mixing promotes dissociation because the $d\sigma_1^*$ orbital involves an antibonding interaction with the pyridine ligand. Stretching the Ru−N_5 bond (*trans* to Ru−N_6) also leads to similar orbital mixing of the tpy π^* orbital and the Ru $d\sigma_1^*$ orbital (Figure 8b). However, the Ru−N_5 bond does not dissociate because the bpy ligand is still tethered by the Ru−N_4 bond. Further elongation of the Ru−N_5 bond results in an increase in energy because of the twisting of the bpy ligand. In contrast to the orbital mixing seen when the Ru−N_5 and Ru−N_6 bonds are stretched, when the Ru−N_4 bond is stretched, the π^* orbital of tpy remains orthogonal to the Ru $d\sigma_2^*$ orbital that corresponds

DOI: 10.1021/acs.inorgchem.7b02398
Inorg. Chem. 2018, 57, 231−240

to $SOMO_2$ of $^3MC_3$, and no mixing occurs (Figure 8c). In addition, the rigidity of the bpy ligand restricts the motion of the Ru−N_4 bond. As a result, the barrier for the transition to the $^3MC_3$ state is high.

CONCLUSIONS

Experimental studies of photoinduced ligand dissociation found that the pyridine ligand is released from $[Ru(tpy)(Me_2bpy)(py)]^{2+}$ significantly more efficiently than from $[Ru(tpy)(bpy)(py)]^{2+}$. To explore the ligand dissociation reaction on the triplet surface, we have calculated the energies and geometries of the ^{3}MLCT and dissociative ^{3}MC states. In comparison to $[Ru(tpy)(bpy)(py)]^{2+}$, the geometry of $[Ru(tpy)(Me_2bpy)(py)]^{2+}$ shows significant strain because of interaction of the methyl groups with the other ligands in both the S_0 and ^{3}MLCT states. Transition to the dissociative ^{3}MC states releases this strain, resulting in lower barriers for ligand dissociation for $[Ru(tpy)(Me_2bpy)(py)]^{2+}$ than for $[Ru(tpy)(bpy)(py)]^{2+}$. By analyzing the molecular orbitals along relaxed scans for stretching the Ru−N bonds, we find that ligand photodissociation is promoted by orbital mixing between the ligand π^* orbital of the ^{3}MLCT state and the dσ^* orbitals that characterize the dissociative ^{3}MC states. Mixing can occur when the Ru−N_6 bond perpendicular to a π-acceptor ligand is stretched and the π^* orbital of tpy and the dσ^* orbital of Ru have good overlap. Orbital mixing results in a smooth and continuous transition from ^{3}MLCT to $^3MC_1$ with a small barrier for photodissociation of the pyridine ligand in $[Ru(tpy)(Me_2bpy)(py)]^{2+}$. In contrast, when the Ru−N_4 bond coplanar with the π-acceptor ligand is stretched, the ligand (tpy) π^* and Ru dσ^* orbitals remain orthogonal; no mixing occurs, and the barrier for the transition from ^{3}MLCT to $^3MC_3$ is high. In addition to orbital mixing, ligand dissociation also depends on the rigidity of the ligand. When the Ru−N_5 bond perpendicular to the π acceptor is stretched, orbital mixing occurs but the bpy group does not dissociate from Ru; instead, bpy twists about its central bond in order to break the Ru−N_5 bond in the $^3MC_2$ state. Nevertheless, stretching of the Ru−N_5 bond followed by elongation of the Ru−N_6 bond can lead to a smaller barrier for transition from ^{3}MLCT to $^3MC_1$, facilitating dissociation of the pyridine ligand. This work provides an understanding of the factors that lead to enhancements in photoinduced ligand dissociation and may be used to predict the structures of complexes for drug photorelease with improved properties.

ASSOCIATED CONTENT

Supporting Information

The Supporting Information is available free of charge on the ACS Publications website at DOI: 10.1021/acs.inorgchem.7b02398.

Higher resolution orbital plots, bond length analysis for the tpy ligand, Ru−N_5 and Ru−N_6 bond distances for relaxed scans of $[Ru(tpy)(Me_2bpy)(py)]^{2+}$, complete citation for the Gaussian program, and Cartesian coordinates for the optimized structures (PDF)

AUTHOR INFORMATION

Corresponding Author

*E-mail for H.B.S.: hbs@chem.wayne.edu.

ORCID

Claudia Turro: 0000-0003-3202-5870

Jeremy J. Kodanko: 0000-0001-5196-7463

H. Bernhard Schlegel: 0000-0001-7114-2821

Notes

The authors declare no competing financial interest.

ACKNOWLEDGMENTS

This work was supported by a grant from the National Science Foundation (CHE1464450). Wayne State University's computing grid provided computational support. J.J.K. and C.T. gratefully acknowledge the National Institutes of Health (R01 EB016072) for its generous support of this research.

REFERENCES

(1) Bayley, H.; Gasparro, F.; Edelson, R. Photoactivatable Drugs. *Trends Pharmacol. Sci.* **1987**, *8*, 138−143.

(2) Knoll, J. D.; Turro, C. Control and utilization of ruthenium and rhodium metal complex excited states for photoactivated cancer therapy. *Coord. Chem. Rev.* **2015**, *282-283*, 110−126.

(3) Ramalho, S. D.; Sharma, R.; White, J. K.; Aggarwal, N.; Chalasani, A.; Sameni, M.; Moin, K.; Vieira, P. C.; Turro, C.; Kodanko, J. J.; Sloane, B. F. Imaging Sites of Inhibition of Proteolysis in Pathomimetic Human Breast Cancer Cultures by Light-Activated Ruthenium Compound. *PLoS One* **2015**, *10*, e0142527.

(4) Respondek, T.; Garner, R. N.; Herroon, M. K.; Podgorski, I.; Turro, C.; Kodanko, J. J. Light Activation of a Cysteine Protease Inhibitor: Caging of a Peptidomimetic Nitrile with Ru-II(bpy)(2). *J. Am. Chem. Soc.* **2011**, *133*, 17164−17167.

(5) Smith, N. A.; Zhang, P. Y.; Greenough, S. E.; Horbury, M. D.; Clarkson, G. J.; McFeely, D.; Habtemariam, A.; Salassa, L.; Stavros, V. G.; Dowson, C. G.; Sadler, P. J. Combatting AMR: photoactivatable ruthenium(II)-isoniazid complex exhibits rapid selective antimycobacterial activity. *Chem. Sci.* **2017**, *8*, 395−404.

(6) Farrer, N. J.; Salassa, L.; Sadler, P. J. Photoactivated chemotherapy (PACT): the potential of excited-state d-block metals in medicine. *Dalton Trans.* **2009**, 10690−10701.

(7) Schatzschneider, U. Photoactivated Biological Activity of Transition-Metal Complexes. *Eur. J. Inorg. Chem.* **2010**, *2010*, 1451−1467.

(8) Howerton, B. S.; Heidary, D. K.; Glazer, E. C. Strained Ruthenium Complexes Are Potent Light-Activated Anticancer Agents. *J. Am. Chem. Soc.* **2012**, *134*, 8324−8327.

(9) Smith, N. A.; Sadler, P. J. Photoactivatable metal complexes: from theory to applications in biotechnology and medicine. *Philos. Trans. R. Soc., A* **2013**, *371*, 20120519.

(10) Mari, C.; Gasser, G. Lightening up Ruthenium Complexes to Fight Cancer? *Chimia* **2015**, *69*, 176−181.

(11) Mari, C.; Pierroz, V.; Ferrari, S.; Gasser, G. Combination of Ru(II) complexes and light: new frontiers in cancer therapy. *Chem. Sci.* **2015**, *6*, 2660−2686.

(12) Lameijer, L. N.; Ernst, D.; Hopkins, S. L.; Meijer, M. S.; Askes, S. H. C.; Le Dévédec, S. E.; Bonnet, S. A Red-Light-Activated Ruthenium-Caged NAMPT Inhibitor Remains Phototoxic in Hypoxic Cancer Cells. *Angew. Chem., Int. Ed.* **2017**, *56*, 11549−11553.

(13) Ryskova, L.; Buchta, V.; Slezak, R. Photodynamic antimicrobial therapy. *Cent. Eur. J. Biol.* **2010**, *5*, 400−406.

(14) Sibata, C. H.; Colussi, V. C.; Oleinick, N. L.; Kinsella, T. J. Photodynamic therapy: a new concept in medical treatment. *Braz. J. Med. Biol. Res.* **2000**, *33*, 869−880.

(15) Zayat, L.; Filevich, O.; Baraldo, L. M.; Etchenique, R. Ruthenium polypyridyl phototriggers: from beginnings to perspectives. *Philos. Trans. R. Soc., A* **2013**, *371*, 20120330.

(16) Karaoun, N.; Renfrew, A. K. A luminescent ruthenium(II) complex for light-triggered drug release and live cell imaging. *Chem. Commun.* **2015**, *51*, 14038−14041.

(17) Zamora, A.; Denning, C. A.; Heidary, D. K.; Wachter, E.; Nease, L. A.; Ruiz, J.; Glazer, E. C. Ruthenium-containing P450 inhibitors for

DOI: 10.1021/acs.inorgchem.7b02398
Inorg. Chem. 2018, 57, 231−240

dual enzyme inhibition and DNA damage. *Dalton Trans.* **2017**, *46*, 2165−2173.
(18) Kovac, A. L. Prevention and treatment of postoperative nausea and vomiting. *Drugs* **2000**, *59*, 213−243.
(19) Kasparkova, J.; Kostrhunova, H.; Novakova, O.; Krikavova, R.; Vanco, J.; Travnicek, Z.; Brabec, V. A Photoactivatable Platinum(IV) Complex Targeting Genomic DNA and Histone Deacetylases. *Angew. Chem., Int. Ed.* **2015**, *54*, 14478−14482.
(20) Huisman, M.; White, J. K.; Lewalski, V. G.; Podgorski, I.; Turro, C.; Kodanko, J. J. Caging the uncageable: using metal complex release for photochemical control over irreversible inhibition. *Chem. Commun.* **2016**, *52*, 12590−12593.
(21) Kang, J.; Lee, S. J. C.; Nam, J. S.; Lee, H. J.; Kang, M. G.; Korshavn, K. J.; Kim, H. T.; Cho, J.; Ramamoorthy, A.; Rhee, H. W.; Kwon, T. H.; Lim, M. H. An Iridium(III) Complex as a Photoactivatable Tool for Oxidation of Amyloidogenic Peptides with Subsequent Modulation of Peptide Aggregation. *Chem. - Eur. J.* **2017**, *23*, 1645−1653.
(22) Respondek, T.; Sharma, R.; Herroon, M. K.; Garner, R. N.; Knoll, J. D.; Cueny, E.; Turro, C.; Podgorski, I.; Kodanko, J. J. Inhibition of Cathepsin Activity in a Cell-Based Assay by a Light-Activated Ruthenium Compound. *ChemMedChem* **2014**, *9*, 1306−1315.
(23) Sgambellone, M. A.; David, A.; Garner, R. N.; Dunbar, K. R.; Turro, C. Cellular Toxicity Induced by the Photorelease of a Caged Bioactive Molecule: Design of a Potential Dual-Action Ru(II) Complex. *J. Am. Chem. Soc.* **2013**, *135*, 11274−11282.
(24) Knoll, J. D.; Albani, B. A.; Durr, C. B.; Turro, C. Unusually Efficient Pyridine Photodissociation from Ru(II) Complexes with Sterically Bulky Bidentate Ancillary Ligands. *J. Phys. Chem. A* **2014**, *118*, 10603−10610.
(25) Knoll, J. D.; Albani, B. A.; Turro, C. Excited state investigation of a new Ru(II) complex for dual reactivity with low energy light. *Chem. Commun.* **2015**, *51*, 8777−8780.
(26) Salassa, L.; Garino, C.; Salassa, G.; Gobetto, R.; Nervi, C. Mechanism of ligand photodissociation in photoactivable [Ru(bpy)(2)L(2)](2+) complexes: A density functional theory study. *J. Am. Chem. Soc.* **2008**, *130*, 9590−9597.
(27) Salassa, L.; Garino, C.; Salassa, G.; Nervi, C.; Gobetto, R.; Lamberti, C.; Gianolio, D.; Bizzarri, R.; Sadler, P. J. Ligand-Selective Photodissociation from [Ru(bpy)(4AP)(4)](2+): a Spectroscopic and Computational Study. *Inorg. Chem.* **2009**, *48*, 1469−1481.
(28) Wagenknecht, P. S.; Ford, P. C. Metal centered ligand field excited states: Their roles in the design and performance of transition metal based photochemical molecular devices. *Coord. Chem. Rev.* **2011**, *255*, 591−616.
(29) Sun, Q. C.; Mosquera-Vazquez, S.; Daku, L. M. L.; Guenee, L.; Goodwin, H. A.; Vauthey, E.; Hausert, A. Experimental Evidence of Ultrafast Quenching of the (MLCT)-M-3 Luminescence in Ruthenium(II) Tris-bipyridyl Complexes via a (3)dd State. *J. Am. Chem. Soc.* **2013**, *135*, 13660−13663.
(30) Camilo, M. R.; Cardoso, C. R.; Carlos, R. M.; Lever, A. B. P. Photosolvolysis of cis-[Ru(alpha-diimine)(2)(4-aminopyridine)(2)](2+) Complexes: Photophysical, Spectroscopic, and Density Functional Theory Analysis. *Inorg. Chem.* **2014**, *53*, 3694−3708.
(31) Greenough, S. E.; Roberts, G. M.; Smith, N. A.; Horbury, M. D.; McKinlay, R. G.; Zurek, J. M.; Paterson, M. J.; Sadler, P. J.; Stavros, V. G. Ultrafast photo-induced ligand solvolysis of cis-[Ru(bipyridine)(2)(nicotinamide)(2)](2+): experimental and theoretical insight into its photoactivation mechanism. *Phys. Chem. Chem. Phys.* **2014**, *16*, 19141−19155.
(32) Ding, L. A.; Chung, L. W.; Morokuma, K. Excited-State Proton Transfer Controls Irreversibility of Photoisomerization in Mononuclear Ruthenium(II) Monoaquo Complexes: A DFT Study. *J. Chem. Theory Comput.* **2014**, *10*, 668−675.
(33) Sun, Q. C.; Mosquera-Vazquez, S.; Suffren, Y.; Hankache, J.; Amstutz, N.; Daku, L. M. L.; Vauthey, E.; Hauser, A. On the role of ligand-field states for the photophysical properties of ruthenium(II) polypyridyl complexes. *Coord. Chem. Rev.* **2015**, *282-283*, 87−99.
(34) Knoll, J. D.; Albani, B. A.; Turro, C. New Ru(II) Complexes for Dual Photoreactivity: Ligand Exchange and O-1(2) Generation. *Acc. Chem. Res.* **2015**, *48*, 2280−2287.
(35) Garcia, J. S.; Alary, F.; Boggio-Pasqua, M.; Dixon, I. M.; Heully, J. L. Is photoisomerization required for NO photorelease in ruthenium nitrosyl complexes? *J. Mol. Model.* **2016**, *22*, 284.
(36) Gottle, A. J.; Alary, F.; Boggio-Pasqua, M.; Dixon, I. M.; Heully, J. L.; Bahreman, A.; Askes, S. H. C.; Bonnet, S. Pivotal Role of a Pentacoordinate (MC)-M-3 State on the Photocleavage Efficiency of a Thioether Ligand in Ruthenium(II) Complexes: A Theoretical Mechanistic Study. *Inorg. Chem.* **2016**, *55*, 4448−4456.
(37) Sun, Q. C.; Dereka, B.; Vauthey, E.; Daku, L. M. L.; Hauser, A. Ultrafast transient IR spectroscopy and DFT calculations of ruthenium(II) polypyridyl complexes. *Chem. Sci.* **2017**, *8*, 223−230.
(38) Tu, Y. J.; Mazumder, S.; Endicott, J. F.; Turro, C.; Kodanko, J. J.; Schlegel, H. B. Selective Photodissociation of Acetonitrile Ligands in Ruthenium Polypyridyl Complexes Studied by Density Functional Theory. *Inorg. Chem.* **2015**, *54*, 8003−8011.
(39) Frisch, M. J.; Trucks, G. W.; Schlegel, H. B.; Scuseria, G. E.; Robb, M. A.; Cheeseman, J. R.; Scalmani, G. B. V.; Mennucci, B.; Petersson, G. A.; Nakatsuji, H.; Caricato, M.; Li, X.; Hratchian, H. P.; Izmaylov, A. F.; Bloino, J.; Zheng, G.; Sonnenberg, J. L.; Hada, M.; Ehara, M.; Toyota, K.; Fukuda, R.; Hasegawa, J.; Ishida, M.; Nakajima, T.; Honda, Y.; Kitao, O.; Nakai, H.; Vreven, T.; Montgomery, J. A.; Peralta, J. E.; Ogliaro, F.; Bearpark, M.; Heyd, J. J.; Brothers, E.; Kudin, K. N.; Staroverov, V. N.; Kobayashi, R.; Normand, J.; Raghavachari, K.; Rendell, A.; Burant, J. C.; Iyengar, S. S.; Tomasi, J.; Cossi, M.; Rega, N.; Millam, J. M.; Klene, M.; Knox, J. E.; Cross, J. B.; Bakken, V.; Adamo, C.; Jaramillo, J.; Gomperts, R.; Stratmann, R. E.; Yazyev, O.; Austin, A. J.; Cammi, R.; Pomelli, C.; Ochterski, J. W.; Salvador, P.; Dannenberg, J. J.; Dapprich, S.; Parandekar, P. V.; Mayhall, N. J.; Daniels, A. D.; Farkas, O.; Foresman, J. B.; Ortiz, J. V.; Cioslowski, J.; Fox, D. J. *Gaussian 09, Revision E.01*; Gaussian, Inc., Wallingford, CT, 2015.
(40) Becke, A. D. Density-Functional Exchange-Energy Approximation with Correct Asymptotic-Behavior. *Phys. Rev. A: At., Mol., Opt. Phys.* **1988**, *38*, 3098−3100.
(41) Perdew, J. P. Density-Functional Approximation for the Correlation-Energy of the Inhomogeneous Electron-Gas. *Phys. Rev. B: Condens. Matter Mater. Phys.* **1986**, *33*, 8822−8824.
(42) Atkins, A. J.; Talotta, F.; Freitag, L.; Boggio-Pasqua, M.; Gonzalez, L. Assessing Excited State Energy Gaps with Time-Dependent Density Functional Theory on Ru(II) Complexes. *J. Chem. Theory Comput.* **2017**, *13*, 4123−4145.
(43) Andrae, D.; Haussermann, U.; Dolg, M.; Stoll, H.; Preuss, H. Energy-Adjusted Abinitio Pseudopotentials for the 2nd and 3rd Row Transition-Elements. *Theor. Chim. Acta* **1990**, *77*, 123−141.
(44) Igelmann, G.; Stoll, H.; Preuss, H. Pseudopotentials for Main Group Elements (Iiia through Viia). *Mol. Phys.* **1988**, *65*, 1321−1328.
(45) Dunning, T. H., Jr.; Hay, P. J. *Modern Theoretical Chemistry*; Plenum: New York, NY, USA, 1976; Vol. 3, pp 1−28.
(46) Francl, M. M.; Pietro, W. J.; Hehre, W. J.; Binkley, J. S.; Gordon, M. S.; Defrees, D. J.; Pople, J. A. Self-Consistent Molecular-Orbital Methods 0.23. A Polarization-Type Basis Set for 2nd-Row Elements. *J. Chem. Phys.* **1982**, *77*, 3654−3665.
(47) Hariharan, Pc; Pople, J. A. Influence of Polarization Functions on Molecular-Orbital Hydrogenation Energies. *Theor. Chim. Acta* **1973**, *28*, 213−222.
(48) Marenich, A. V.; Cramer, C. J.; Truhlar, D. G. Universal Solvation Model Based on Solute Electron Density and on a Continuum Model of the Solvent Defined by the Bulk Dielectric Constant and Atomic Surface Tensions. *J. Phys. Chem. B* **2009**, *113*, 6378−6396.
(49) Dennington, R.; Keith, T.; Millam, J. M. *GaussView, version 5*; Semichem, Inc., Shawnee Mission, KS, USA, 2009.
(50) Neese, F. Definition of corresponding orbitals and the diradical character in broken symmetry DFT calculations on spin coupled systems. *J. Phys. Chem. Solids* **2004**, *65*, 781−785.

DOI: 10.1021/acs.inorgchem.7b02398
Inorg. Chem. 2018, 57, 231−240